NUMERICAL STUDY OF DROPLET VAPORIZATION AND COMBUSTION AT HIGH PRESSURE AND HIGH TEMPERATURE

J.-Y. KOO[1]* and J.-B. KO[2]

[1]School of Aerospace and Mechanical Engineering, Hankuk Aviation University, Gyeonggi 412-791, Korea
[2]Graduate School, Hankuk Aviation University, Gyeonggi 412-791, Korea

ABSTRACT–A numerical study of high pressure and temperature droplet vaporization and combustion is conducted by formulating one dimensional evaporation model and single-step chemical reaction in the mixture of hydrocarbon fuel and air. The ambient pressure ranged from atmospheric conditions to the supercritical conditions. In order to account for the real gas effect on fluid p-v-T properties in high pressure conditions, the modified Soave-Redlich-Kwong state equation is used in the evaluation of thermophysical properties. Some computational results are compared with Sato's experimental data for the validation of calculations in case of vaporization. The comparison between predictions and experiments showed quite a good agreement. Droplet surface temperature increased with increasing pressure. Ignition time increased with increasing initial droplet diameter. Temporal or spatial distribution of mass fraction, mass diffusivity, Lewis number, thermal conductivity, and specific heat were presented.

KEY WORDS : Droplet vaporization and combustion, Droplet surface temperature, Ignition time, Thermal conductivity

1. INTRODUCTION

Vaporization of liquid fuel, and the subsequent mixing between air and fuel species are key issues in the development of liquid-fueled combustion devices such as diesel, gas turbine, and liquid-propellant rocket engines. In the combustion of power generation and propulsion applications, the burning rate is controlled by the vaporization of liquid fuel because the chemical reaction rates during main combustion period are so high comparing vaporization rates. In the past few decades, combustor performance has been substantially enhanced by increasing the operating temperature and pressure in the thermodynamic supercritical regime of fuel species.

The understanding of droplet vaporization in supercritical environments is essential in liquid–fueled combustion devices such as Diesel engines, gas turbines, and liquid rocket engines. Several theoretical works have been conducted for understanding of droplet vaporization and combustion under high pressure conditions. Manrique and Borman (1969) initiated a systematic treatment of droplet vaporization at near-critical based on a quasi-steady model. Vaporization mechanisms were significantly modified by the effects of thermodynamic non-idealities, property variations, and high-pressure corrections for phase equilibrium.

A series of experimental and theoretical studies on droplet combustion in both stagnant and forced convective environments were conducted by Lazar and Faeth (1971); Lee *et al.* (2001) and Canada and Faeth (1973). Numerical techniques to simulate high-pressure droplet vaporization and combustion have employed by Hsieh *et al.* (1991), Curtis and Farrel (1992), and Delpanque and Sirignano (1993). All of these models, however, adopted certain rudimentary assumptions and empirical formulas for fluid properties that were extrapolated from low-pressure cases, with their accuracy for high-pressure applications subject to question. Furthermore, no effort was made to treat the thermodynamic phase transition through the critical point. In order to remedy these deficiencies, a series of fundamental studies were conducted using the state-of-art treatment of thermodynamic and transport phenomena by Yang *et al.* (1994) and Lafon *et al.* (1995). Extensive reviews of supercritical vaporization were recently given by Bellan (2000) and Yang (2000).

In this study, droplet vaporization and combustion at various ambient pressures is studied numerically by formulating one dimensional evaporation model and single-step chemical reaction in the mixture of n-heptane and air. A droplet vaporization and combustion which is placed in a supercritical ambient conditions is different from conventional low ambient conditions. At high pressure conditions, especially supercritical pressures, a droplet is heated up and finally reaches the critical point,

---

then the transient effect is important. After that, a sharp distinction between the liquid and gaseous phases disappears because the heat of vaporization and surface tension becomes zero. The droplet is treated as the dense fluid instead of liquid in the supercritical conditions. High-pressure phase equilibrium is assumed at droplet surface. Non-ideal thermodynamic and transport property at near critical and supercritical conditions are also considered.

2. THEORETICAL FORMULATION AND BOUNDARY CONDITIONS

The evolution of the flow for a single fuel droplet exposed to a quiescent air environment is described by writing down the balance equations with the above assumptions.

1) Mass conservation

$$\frac{d}{dt} \int_{V(t)} \rho dV + \int_{A_a(t)} \rho(\vec{v} - \vec{v}_s) \cdot d\vec{A} = 0 \tag{1}$$

2) Momentum conservation

$$\nabla p = 0$$

3) Energy conservation

$$\frac{d}{dt} \int_{V(t)} \rho e_t dV + \int_{A_a(t)} \rho e(\vec{v} - \vec{v}_s) \cdot d\vec{A} =$$
$$- \int_{A_a(t)} \vec{q}_e \cdot d\vec{A} - \int_{A_a(t)} p\vec{v} \cdot d\vec{A} \tag{2}$$

4) Species conservation

$$\frac{d}{dt} \int_{V(t)} \rho Y_i dV + \int_{A(t)} \rho Y_i(\vec{v} - \vec{v}_s) \cdot d\vec{A} =$$
$$- \int_{A_a(t)} \vec{q}_i \cdot d\vec{A} + \int_{V(t)} \dot{w}_i \cdot d\vec{A} \tag{3}$$

where the surface and volume integrations are carried out over a finite spherical control volume concentric with the droplet. The physical variables ρ, $\vec{v}$, e_t, p, Y_i and $\dot{w}_i$ are density, velocity, specific total internal energy, pressure, mass fraction, and rate of production of species i, respectively. $\vec{v}_s$ is the moving velocity of the control surface. V and A_a are the control volume and control surface area. The specific total internal energy is the sum of internal energy and kinetic energy.

The diffusive flux terms, $\vec{q}_e$ and $\vec{q}_i$ are determined by Fourier's and Fick's Laws, respectively.

$$\vec{q}_i = \rho Y_i \vec{v}_i = -\rho D_{im} \nabla Y_i \tag{4}$$

where $\vec{v}_i$ is the velocity of species i. D_{im} is the effective mass diffusivity of species i in the mixture, which can be related to the binary mass diffusivity (D_{ij})

$$D_{im} = (1 - x_i) / \sum_{i \neq j}^{N} (x_j / D_{ij}) \tag{5}$$

Energy diffusion consists of the thermal conduction term and mass diffusion term.

$$\vec{q}_e = -\lambda \nabla T - \sum_{i=1}^{N} \vec{q}_i \bar{h}_i \tag{6}$$

where λ is thermal conductivity, and $\bar{h}_i$ is the partial mass enthalpy of species i.

A uniform temperature is initially prescribed inside the droplet, and there is no fluid flow and no gaseous species. The initial gaseous temperature is also assumed to be uniform, and there is no velocity and no fuel species in the gaseous phase,

At droplet surface, the conventional assumption of thermodynamic phase equilibrium holds, resulting in the equality of temperature, pressure, and chemical potentials between the two phases. Accordingly, the equilibrium mass fractions in both sides can be calculated.

Spherical symmetry boundary conditions remain at the droplet center. Outside boundary is maintained at a distance of 100 times of the droplet radius from the droplet center. All the variables there will not be affected by droplet vaporization and remain at their initial values.

The system is closed and devoid of chemical reaction, and there is therefore conservation of mass for each consitituent for the Gibbs free energy minimization.

$$\sum_{i=1}^{N} (\mu_i^l dm_i^l) + \sum_{i=1}^{N} (\mu_i^g dm_i^g) = 0 \tag{7}$$

This being represented by,

$$dm_i^l = -dm_i^g \tag{8}$$

$$\sum_{i=1}^{N} (\mu_i^l - \mu_i^g) dm_i = 0 \tag{9}$$

Prior to the occurrence of the critical mixing state, thermodynamic liquid/vapor phase equilibrium is assumed to prevail at the droplet surface. Temperatures, pressures, and chemical potentials at both sides of the surface must be equal,

$$T^g = T^l$$
$$p^g = p^l \tag{10}$$
$$\mu_i^g = \mu_i^l$$

Phase change occurs at droplet surface, where undergo rapid heat and mass transfer. The conservation of mass, species and energy across the interface are

$$\dot{m} = \rho(\vec{v} - \dot{R}) \cdot \vec{A}\big|_{r=R_+} = \rho(\vec{v} - \dot{R}) \cdot \vec{A}\big|_{r=R_-} \tag{11}$$

$$\dot{m}_l = [\dot{m}Y_i + \vec{q}_i \cdot \vec{A}]_{r=R_+} = [\dot{m}Y_i + \vec{q}_i \cdot \vec{A}]_{r=R_-} \tag{12}$$

$$-\lambda \nabla T\big|_{r=R_-} = -\lambda \nabla T\big|_{r=R_+} + \sum_{i=1}^{N} \dot{m}_i(\bar{h}_i^g - \bar{h}_i^l) \tag{13}$$

where R_- and R_+ denotes the conditions at the

interface on the interface on the liquid side and gaseous side, respectively. $\dot{R}$ is the droplet regression rate, $\dot{m}$ the mass vaporization rate, and $\dot{m}_i$ the vaporization rate of species i.

In the high pressure conditions, the modified SRK equation of state is considered to be both simple and fairly accurate, which takes the following form (1978):

$$p = \frac{\rho R_u T}{(W - b\rho)} - \frac{a\alpha}{W} \frac{\rho^2}{(W + b\rho)} \tag{14}$$

where R_u is the universal gas constant. The parameters 'a' and 'b' account for the effects of the attractive and repulsive forces between molecules, respectively. 'α' is the third parameter, which is a function of temperature and acentric factor.

The mixing law are deduced from the construction of the equation and especially from the determination of the coefficients 'a' and 'b'. Since 'b' was introduced as being the limit volume at infinite pressure, a near-universal experimental finding, its dependence on composition is obvious and molecular theory gives a second virial coefficient as a second-degree function of the compositions for 'a'.

$$\frac{b\rho}{M} = \sum_i \frac{b_i \rho_i}{M_i} \tag{15}$$

$$a = \sum_i \sum_j X_i X_j a_{ij} \tag{16}$$

Where X is molefraction of species of i and j.

A single-step chemical reaction is adopted for the combustion of hydrocarbon fuel droplet. Fuel is assumed to react with air stoichiometrically.

$$C_x H_y + \left(x + \frac{y}{4}\right)(O_2 + 3.76N_2) \rightarrow$$
$$\frac{y}{2}H_2O + xCO_2 + 3.76\left(x + \frac{y}{4}\right)N_2 \tag{17}$$
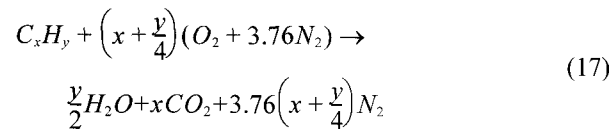
The rate of production of each species is calculated using the single-step, global reaction mechanism suggested by Westbrook and Dryer (1981).

$$\dot{w}_{fuel} = -A W_{fuel} \exp(-E_a/R_u T)[fuel]^a [O_2]^b \tag{18}$$

$$\dot{w}_{O_2} = -\left(x + \frac{y}{4}\right)\left(\frac{W_{O_2}}{W_{fuel}}\right)\dot{w}_{fuel} \tag{19}$$

$$\dot{w}_{CO_2} = -x\left(\frac{W_{CO_2}}{W_{fuel}}\right)\dot{w}_{fuel} \tag{20}$$

$$\dot{w}_{H_2O} = -\frac{y}{2}\left(\frac{W_{H_2O}}{W_{fuel}}\right)\dot{w}_{fuel} \tag{21}$$

where the parameters A, E_a, a, b have been chosen as 5.1×10^{11} cm³/gmol-s, 30,0 kcal/gmol, 0.25, and 1.5, respectively Turns (1996).

3. NUMERICAL METHODS

The conservation equations are discretized on a time varying grid with a finite volume formulation and solved using a fully implicit scheme. Two different scenarios occur depending upon whether the vaporization regime is subcritical or supercritical. However, in both cases the grid follows the time regression of droplet interface. For supercritical regimes the droplet interface is defined by critical isotherm line. To perform a fully implicit treatment of the problem using time-varying grid cell, the volume of each grid cell is included in the quantities computed at each time step by inversion of the linear system introduced by the implicit formulation. If the location of each grid node is only a function of the instantaneous droplet radius, then the volume variation of each grid cell may be easily linked to the volume variations of the adjacent cells, same thing for the surface velocities. The independent variables in this work are defined as

$$Q = (\rho V, \rho v A, \rho e V, \rho Y_i V, V)^T \tag{22}$$
$$i = 1, \ldots, N{-}1$$

Where N, V, A, and $\vec{v}$ are total number of species, control volume, area of the control surface, and velocity of control surfaces respectively. Pressure and temperature are determined from these variables. All the quantities required in the resolution are expressed with those contained in the previous vector using a linearization technique. The volume V is chosen to be a variable since it varies with time in the present moving boundary problem. Its movement is governed by the following equation:

$$\frac{d}{dt} \int_{V_a(t)} dV - \int_{A_a(t)} \vec{v} \cdot d\vec{A} = 0 \tag{23}$$

For application of the implicit scheme, all the variables in the discretized governing equations need to be linearized and related to the independent variables shown in Equation (22). The temperature T at a new time step n+1 can be expressed as

$$T^{n+1} = T^n + \left(\frac{dT}{dQ}\right)\Delta Q = T^n + \left(\frac{dT}{dQ}\right)(Q^{n+1} - Q^n) \tag{24}$$

To estimate the high pressure and high temperature conductivity, we use the experimental correlation resulting from the work of Stiel and Thodos.

$$(\lambda_m - \lambda_m^0)\Gamma_m Z_{Cm}^5 = A(e^{B\rho_{rm}} - 1) \tag{25}$$

Where $\Gamma = \dfrac{T_{cm}^{1/6}}{P_{cm}^{2/3} M_m^{1/2}}$, A and B are constant variables.

4. RESULTS AND DISCUSSION

The adopted hydrocarbon fuel is n-heptane and the surrounding gas is air which is assumed to be consist of 21% oxygen and 79% nitrogen. The liquid n-heptane is initially at 300 K in the high ambient temperatures which ranges from 450 K to 1500 K. The reference initial droplet diameter is 150 μm. The ambient pressures are also varied.

The calculation for the combustion is conducted until the droplet diameter is 10% of the initial droplet diameter. When the diameter is 10% of the initial diameter, the mass is about 0.1% of the initial mass. The time when the mass reaches at 0.1% of the initial mass, it is considered as lifetime of the droplet combustion. Table 1 shows the critical conditions of n-heptane, air (oxygen and nitrogen), and products.

Figure 1 shows the temporal variations of the dimensionless droplet diameter at pressures of 0.1, 0.5 and 2.0 MPa, and an ambient temperature of 468, 648 and 660 K. At the beginning of the vaporization process, both the experimental and computational results agree quite well and show droplet expansion due to the sudden heating of the droplet. The reasonably good agreement of the droplet vaporization rate between the numerical and

experimental results before t/d_0^2 is less than about 1.5 validates the numerical model developed in this study. However, after t/d_0^2 is larger than about 1.5, there are some discrepancies between the numerical and experimental results, but with same trend between the numerical results and the experimental results. The discrepancies may come from the following reasons. First, some uncertainties remain in the value of the initial droplet temperature in the experiment, which is strongly affected by the ambient temperature because of the droplet formation technique used. Moreover Vielli et al. (1996) demonstrated that the microgravity conditions obtained in the drop tower and parabolic flight experiments could not completely avoid the buoyancy effect on droplet vaporization rate, which increases with the increase of pressure. In addition to this, considering pure vaporization conditions leads to droplet lifetime of the order of 10 to 30 for the dropletsize handled experimentally. On the other hand, micro-gravity test facilities provide micro-gravity conditions for a much shorter amount of time. Nomura et al. (1996) and Sato (1993) has conducted droplet vaporization experiments under micro-gravity conditions. Second, in the Nomura et al.'s experiments (1996), 0.6–0.8 mm droplets were suspend-

Table 1. Critical Properties of the Species in the Heptane/ Air system.

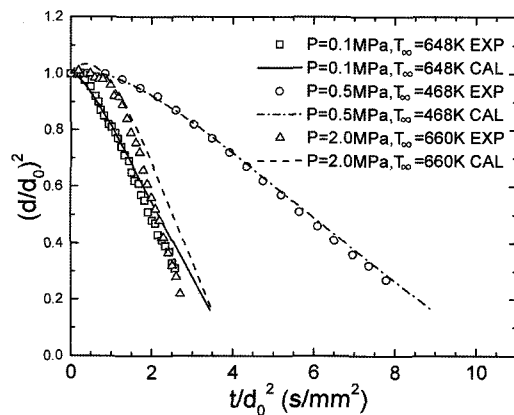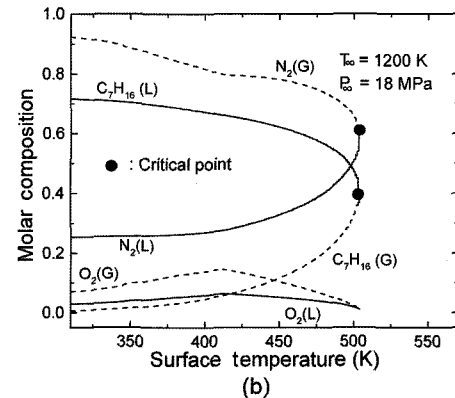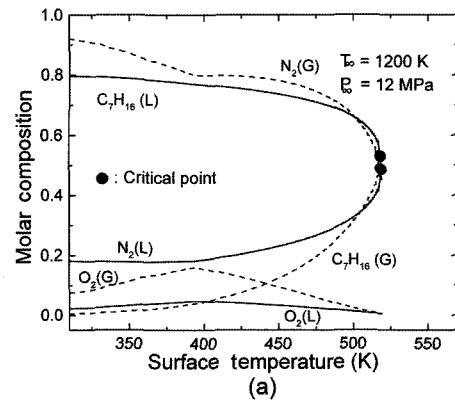| Species	M_w (g/mole)	T_c (K)	P_c (MPa)	V_c (cm³/mole)
C_7H_{16}	100	540.3	2.74	432.0
N_2	28	126.2	3.39	89.8
O_2	31	154.6	5.04	73.4
CO_2	44	304.1	7.38	93.9
H_2O	18	647.3	22.12	57.1

Figure 1. Comparison of normalized droplet diameter versus time between calculated and experimental data.

Figure 2. Surface molar composition histories versus surface temperature: (a) P_∞=12 MPa; (b) P_∞=18 MPa.
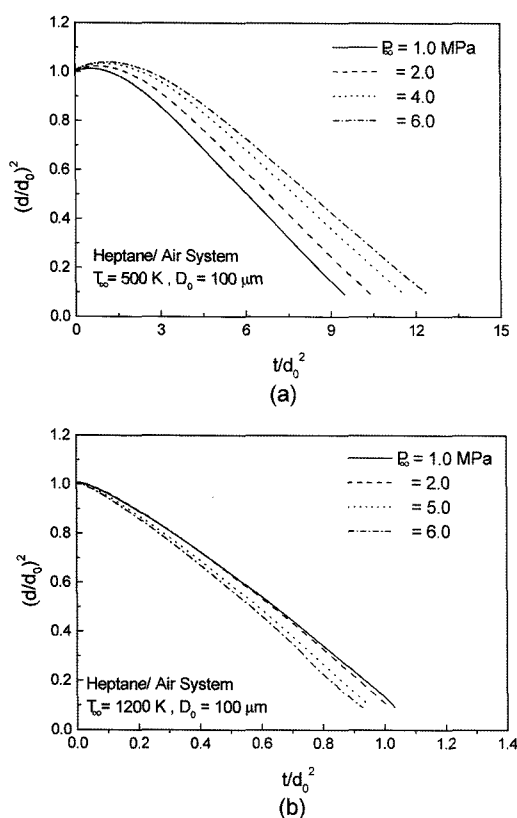
Figure 3. Temporal histories of droplet diameter for heptane/air system at different ambient pressures: (a) Subcritical condition; (b) Supercritical condition.

ed from a vaporization. The effect of suspension fiber on the droplet vaporization rate increases with the increase of pressure and temperature, and with the decrease of droplet size. The fiber in the experiments accelerates the droplet vaporization at the end of its lifetime. This might lead to significant difference between numerical predictions and experimental results at high ambient pressure conditions.

Figure 2 shows the surface composition history of n-heptane/air system as a function of surface temperature for two ambient pressures, respectively $p = 12$ and 18 MPa. As surface temperature increases, both liquid and gaseous oxygen compositions at the interface become smaller. A raise of surface temperature is linked with an increase of n-heptane gaseous composition, that is a decrease of nitrogen gaseous composition.

Figure 3 shows the temporal histories of the droplet diameter squared at various pressures. The droplet lifetime is decreased with increasing ambient pressures at supercritical temperature condition but droplet lifetime is increased with increasing ambient pressure at subcritical temperature condition. There is a heat-up period at the start of the process before ignition where the droplet is
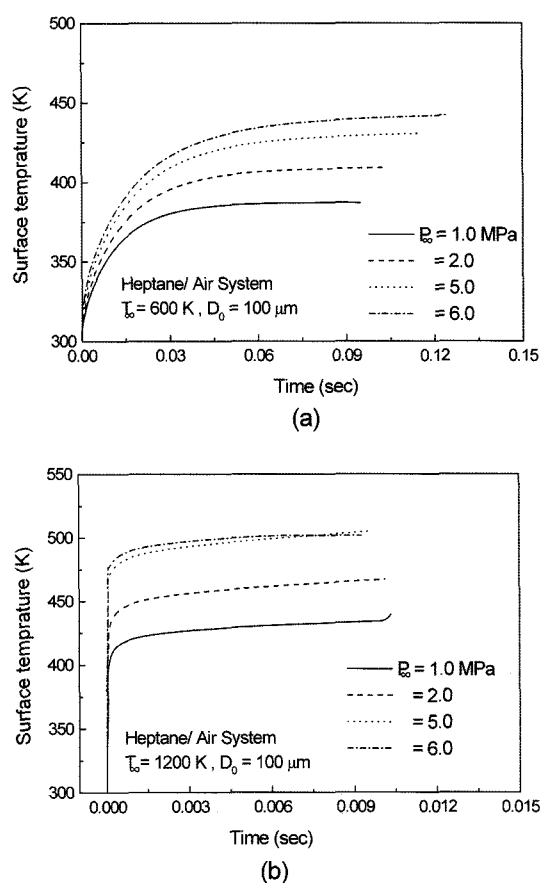

Figure 4. Temporal variation of droplet surface temperature for heptane/air system at different ambient pressures: (a) Subcritical condition; (b) Supercritical condition.

greater than the initial one because the volume of droplet expansion is greater than that of vaporization. During heat-up process, some part of the heat reaching at the droplet surface is used to vaporize liquid fuel, other part of the heat is conducted into the droplet interior for droplet heating.

Figure 4 shows temporal variation of droplet surface temperature at various pressure which ranges from subcritical pressures to supercritical pressures. The temperature of droplet surface at subcritical temperature condition rises gradually but it rises up very rapidly at the initial time due to the ignition of the fuel. The temperature of droplet surface rises up very rapidly at the initial time due to the ignition of the fuel. Ignition time is defined as the time when surface temperature is saturated. Ignition time increases with increasing pressure because of increase of density with increasing pressure. Surface temperature also increase with increasing pressure because of increase of density and molefraction of activitive fuel and oxygen with increasing pressure.

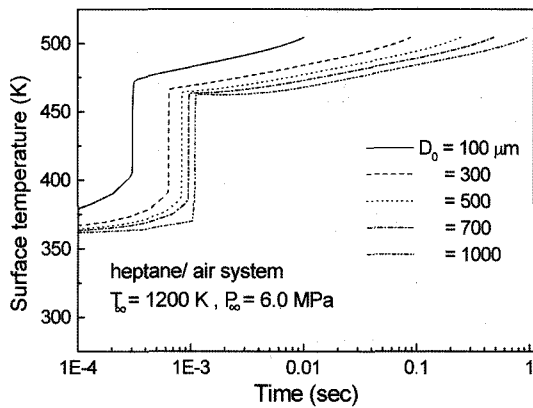Figure 5 shows temporal variation of droplet surface

Figure 5. Temporal variation of droplet surface temperature for heptane/air system at different initial diameters.
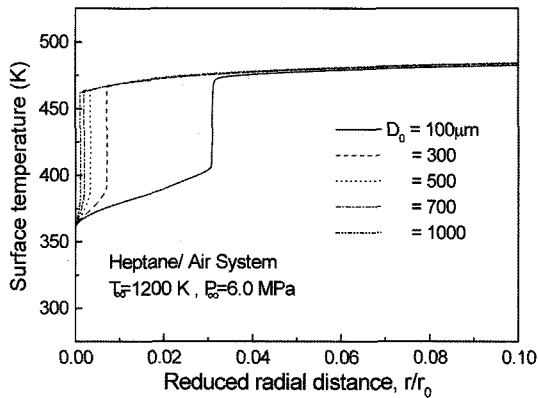

Figure 7. Radial profiles of temperature for heptane/air system at different times.

Figure 6. Temporal variation of droplet surface temperature for heptane/air system at different initial diameters.

Figure 8. Radial profiles of mass fraction for species in heptane/air system at 4.1 ms.

temperature at various initial droplet diameter. Figure 6 shows temporal variation of droplet surface versus t/D_0^2 for various initial droplet sizes. Ignition time increases with initial droplet sizes as shown in Figure 5, but the d-squared law for the ignition time is not valid, which can be seen in Figure 6.

Figure 7 shows temperature profiles versus reduced radial distance for heptane/air system at different times. The peak point of temperature might be the place where stoichiometric reaction occurs. It can be seen in Figure 7 that flame is propagated toward outside and heat is transferred into the inside of liquid droplet with increasing time. The initial liquid temperature is 300 K and the temperature of inside liquid fuel at 8.08 ms is 500 K.

Figure 8 shows radial profiles of mass fraction for species in heptane/air system at 4.1 ms. Fuel and oxygen is completely consumed and mass fraction is zero at certain radial position where the fuel-air ratio is stoichiometric while the mass fraction of products peaks.

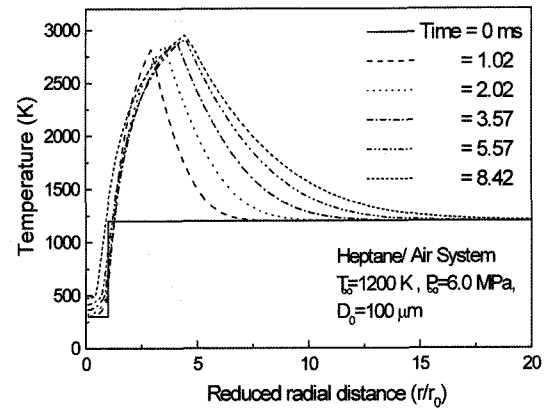Figure 9 shows the radial profiles of mass fraction of

Figure 9. Radial profiles of mass fraction for heptane and oxygen at different times.
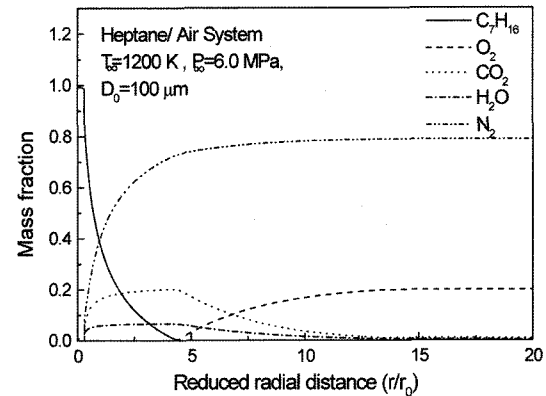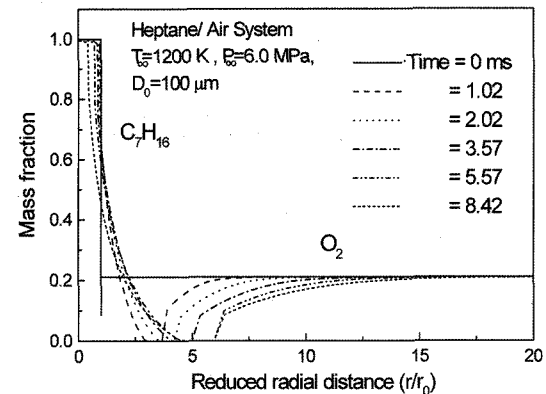
n-heptane/air system at different times. Flame is propagated toward outside because the stoichiometric reaction point moves outward with increasing time. The radius of droplet surface is decreasing because the mass fraction of
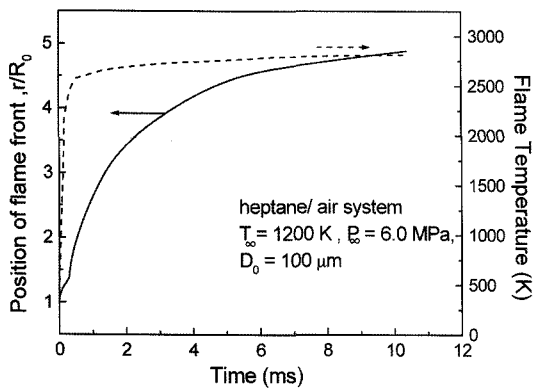
Figure 10. Temporal profiles of flame position and temperature for heptane/air system.
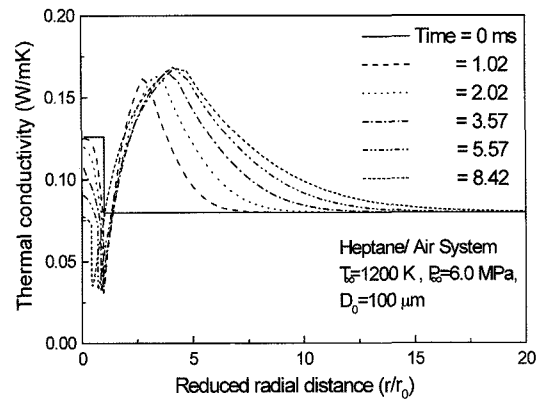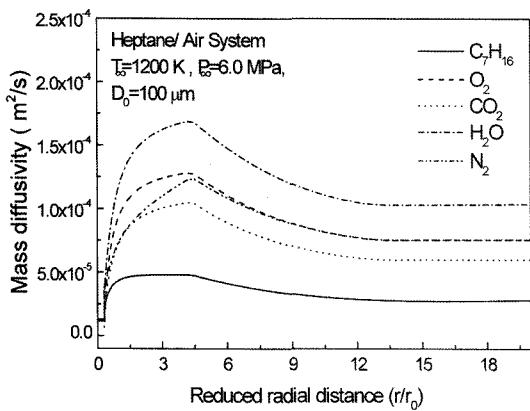

Figure 11. Radial profiles of mass diffusivity for species in heptane/air system at 8.08 ms.
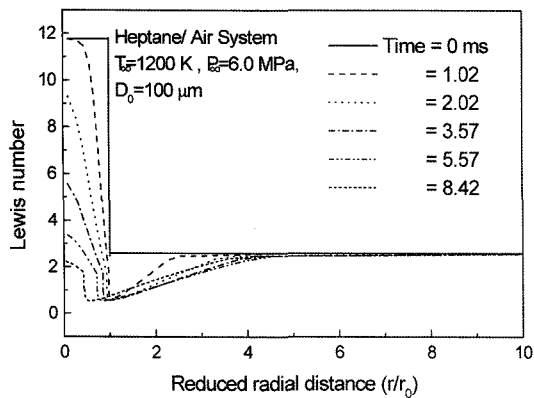

Figure 12. Radial profiles of Lewis number for heptane/air system at different times.

fuel is decreasing with increasing time.

Figure 10 shows temporal profiles of flame position and its temperature for heptane/air system.

Figure 11 shows radial profiles of mass diffusivity for

Figure 13. Radial profiles of thermal conductivity for heptane/air system at different times.

species in heptane/air system at 8.08 ms. Mass diffusivity is proportional to temperature and inversely proportional to molecular weight. Species with higher molecular weight indicate lower mass diffusivity in Figure 11. The profile of mass diffusivity in Figure 11 is similar as the temperature profile which is shown in Figure 7. Mass diffusivity sharply rises up to the interface which is reaction zone and decrease after reaction zone.

Figure 12 shows radial profiles of Lewis number for heptane/air system. Lewis number of mixture characterize the ratio of thermal diffusivity to mass diffusivity of mixture. Lewis number provides the indication of what process controls phenomena. For example, if Lewis number is order of one, it means that thermal diffusion and mass diffusion occur at similar rates. If Lewis number is greater than order of 10, it means that thermal diffusion is faster than mass diffusion. The drop of Lewis number at the vicinity of the interface is results from the dissolution of nitrogen into liquid fuel and phase transition from liquid to vapor. Lewis number decreases with time.

Figure 13 shows the radial profiles of thermal conductivity for heptane/air system at different times. Liquid fuel has a higher thermal conductivity than gas phase material. Dissolution of nitrogen gas into liquid fuel and liquid/gas phase transition result in a sharp drop in thermal conductivity at the interface. A sharp jump can be seen at the reaction zone where temperature increases sharply because thermal conductivity is proportional to the temperature. Thermal conductivity at the center of liquid fuel decreases with time because more dissolved gas can easily reach the center of droplet with decreasing of droplet size.

5. CONCLUSIONS

From one dimensional vaporization model and single-

step chemical reaction model in the mixture of n-heptane, the followings can be concluded.

(1) The effect of ambient pressure and initial droplet size on the droplet characteristics such as droplet lifetime and surface temperature was investigated. Droplet lifetime was decreased and surface temperature was increased with increasing ambient pressure. Ignition time was increased with increasing pressure because of increase of density with increasing pressure. Ignition time was increased with initial droplet sizes ranging from 100 μm to 1000 μm but the d-squared law for the ignition time is not valid. The surface temperature versus t/D_0^2 is almost constant irrespective of initial droplet sizes.

(2) The radial profiles of thermo-physical properties were investigated at different times and at 1200 K and 6.0 MPa. Lewis number and thermal conductivity were sharply dropped at the interface of liquid and gas phase because more energy was used to the change of phases. Thermal conductivity at the center of liquid fuel was decreased with time because more dissolved gas can easily reach the center of droplet with decreasing of droplet size.

REFERENCES

Bellan, J. (2000). Supercritical (and Subcritical) fluid behavior and modeling: drops, streams, shear and mixing layers, jets, and spray. *Progress in Energy and Combustion Science*, **26**, 329–366.

Canada, G. S. and Faeth, G. M. (1973). Fuel droplet burning rates at high pressures. *Proc. 14th Symp. (Int.) on Combustion*, 135–1354.

Curtis, E. W. and Farrel, P. V. (1992). A numerical study of high-pressure droplet vaporization. *Combustion and Flame*, **90**, 85–102.

Delplanque, J. P. and Sirignano, W. A. (1993). Numerical study of the transient vaporization of an oxygen droplet at sub- and super-critical conditions. *Int. J. Heat and Mass Transfer* **36**, 2, 303–314.

Graboski, M. S. and Daubert, T. E. (1978). A modified soave equation of state for phase equilibrium calculation, 1. hydrocarbon Systems. *Industrial and Engineering Chemistry Process Design and Development* **17**, 4, 443–448.

Hsieh, K. C., Shuen, J. S. and Yang, V. (1991). Droplet vaporization in high-pressure environments I: Near

critical conditions. *Combustion Science and Technology*, **76**, 111–132.

Lafon, P. (1995). Modélisation et Simulation Numérique de L'Evaporation et de la Combustion de Gouttes à Haute Pression, Ph.D Dissertation, à L'Université D'Orléans.

Lazar, R. S. and Faeth, G. M. (1971). Bipropellant droplet combustion in the vicinity of the critical point. *Proc. 13th Symp. (Int.) on Combustion*, 801–811.

Lee, M. J., Kim, Y. W., Ha, J. Y. and Chung, S. S. (2001). Effects of watery vapor concentration on droplet evaporation in hot environment. *Int. J. Automotive Technology* **2**, 3, 109–115.

Manrique, J. A. and Borman, G. L. (1969). Calculations of steady state droplet vaporization at high ambient pressures. *Int. J. Heat and Mass Transfer*, **12**, 1081–1095.

Morin, C., Chauveau, C. and Gökalp, I. (2000). Vaporization of n-alkane droplet at high temperature and pressure. *8th Int. Conf. Liquid Atomization and Spray System*, Pasadena, CA, USA.

Nomura, H., Ujiie, Y., Rath, H. J., Sato, J. and Kono, M. (1996). Experimental study on high pressure droplet evaporation using microgravity conditions. *26th Symp. (Int.) on Combustion, The Combustion Institute*, 1267–1273.

Reid, R. C., Prausniz, J. M. and Sherwood, T. K. (1977). Thermal conductivies of gas mixtures at high pressures. *The Properties of Gases and Liquids*, 10.35–10.38.

Sato, J. (1993). Studies on droplet evaporation and combustion in high pressures. *AIAA Paper* 93–0813.

Stephen R. Turns. (1996). *An Introduction to Combustion*. MacGraw-Hill. Singapore. Int. Edn.. 135–137.

Vielle, B., Chauveau, C., Chesnau, X., Odeïde, A. and Gökalp, I. (1996). High pressure droplet burning experiments in microgravity. *26th Symp. (Int.) on Combustion*, 259–1265.

Westbrook, C. K. and Dryer. F. L. (1981). Simplified reaction mechanisms for the oxidation of hydrocarbon fuels in flames. *Combustion Science and Technology*, **27**, 31–43.

Yang, V. (2000). Modeling of supercritical vaporization, mixing, and combustion processes in liquid-fueled propulsion system. *28th Symp. (Int.) on Combustion*, 925–942.

Yang, V., Lin, N. N. and Shuen, J. S. (1994). Vaporization of liquid oxygen (LOX) droplets in supercritical hydrogen environments. *Combustion Science and Technology*, **97**, 247–270.